Efficient Microwave-Assisted Extraction of Nitrites from Cured Meat and their Voltammetric Detection at Chemically Modified Electrodes based on Hexamethyl-p-Terphenyl Poly(methylatedbenzimidazolium) incorporating Nitrogen-doped Graphite Nanoplatelets

Sandra Hernandez-Aldave,[a §] Afshin Tarat,[b] and Paolo Bertoncello,[a, *]

[a] Department of Chemical Engineering, Faculty of Science and Engineering, Swansea University, Bay Campus, Crymlyn Burrows, Swansea SA1 8EN, United Kingdom
[b] Perpetuus Advanced Materials, Unit B1, Olympus Court, Millstream Way, Swansea Vale, Llansamlet, SA7 0AQ, United Kingdom
[§]Current address: Department of Chemical Sciences, School of Applied Sciences, University of Huddersfield, HD1 3DH, United Kingdom

Supporting Informations

S1

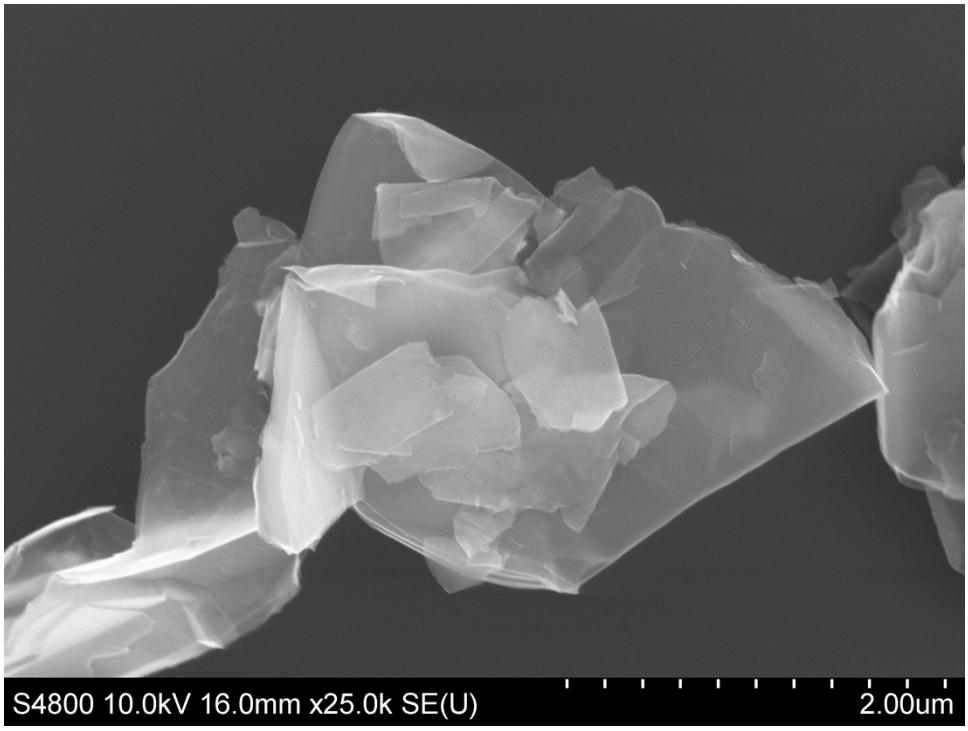

Figure S1. A 2 μm-fold magnification field-emission scanning electron micrograph of NGNPs.

S2

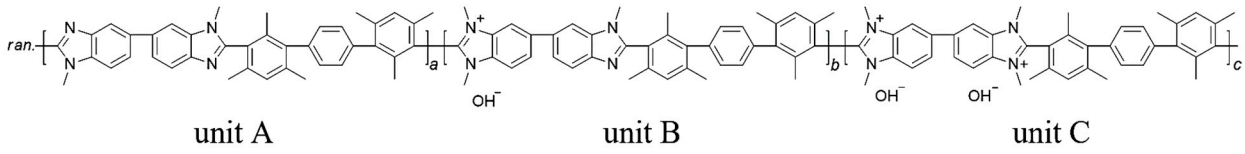

Figure S2. Structure of HMT-PMBI [hexamethylterphenyl=HMT; poly(methylated benzimidazolium) = PMBI] in hydroxide form for those with a degree of methylation (dm) between 50% and 100%.

S3 (a). Procedure of Extraction and detection of nitrite ions from meat products using the ISO 2918:1975 Method.

200 g of meat were minced and homogenized. A 10-g sample of minced meat was then mixed with 5 mL of an aqueous saturated borax solution (0.05 g/mL of disodium tetraborate decahydrate) were added. Then, 100 mL of hot water (70 °C) was incorporated to the sample solution solution, which was heated in a boiling water bath for 15 min, while the solution was repeatedly agitated. The solution was then allowed to cool to room temperature, before adding 2 mL of 0.29 mol/L of potassium ferrocyanide trihydrate and 2 mL of 1.2 mol/L zinc acetate dihydrate containing 3% (v/v) glacial acetic acid. The total solution was mixed thoroughly after each addition. The final solution was transferred into a 200 mL volumetric flask, diluted with deionized water and mixed. The homogenized solution was left to rest for 30 minutes at room temperature. After 30 minutes, the supernatant liquid was decanted and filtered using a fluted filter paper (free of nitrite) until a clear solution was obtained. An aliquot of the filtrated sample (typically not more than 25 mL) was added to a 100 mL volumetric flask where deionized water was added until a total volume of about 60 mL is obtained. Separately, a solution defined as Solution I was prepared by dissolving 2 g of sulfanilamide in 800 mL of deionized water. This sulfanilamide solution was then cooled down, filtered, before 100 mL of concentrated hydrochloric acid was added with stirring. Finally, solution I was diluted with deionized water up to a final volume of 1000 mL. Solution II was prepared dissolving 0.25 g of N-1-naphthylethylenediamine dihydrochloride (NED) in 250 mL of water. The resulting solution was stored in a well-stoppered brown bottle and left in the refrigerator at 4°C. Subsequently, 10 mL of solution I and 6 mL of 44.5 % (v/v) of hydrochloric acid solution were added and mixed. The final solution was left for 5 minutes in the dark at room temperature before adding Solution II. After 5 minutes, 2 mL of Solution II were added, mixed and left for 10 minutes until a purple/blue color developed. The final colored solution was diluted to 100 mL with deionized water. The absorbance of the sample was measured at 538 nm against a reagent blank using a UV instrument and a cuvette of 1 cm optical path length [1]. The nitrite content of the samples, expressed as milligrams of sodium nitrite per kilogram of meat, was calculated following the Beer's law, from a similarly prepared calibration graph using the formula:

$$\mathrm{NaNO_2} = c \times \frac{2000}{m \times V}$$

where: *m* is the mass in grams, of the sample; *V* is the volume, in mL, of the aliquot for the UV measurement taken from the filter sample; *c* is the concentration of nitrites in µg/mL, obtained from the calibration plot.

S3 (b). Procedure of Extraction and detection of nitrite ions from meat products using the AOAC Method 973.31

Bacon meat (5 g) were minced and transferred into a 50 mL beaker. Hot deionized water was added, and the lumps were broken down with a glass rod. Afterwards, 300 mL of deionized water was added to the sample, transferred to a 500 mL volumetric flask and the homogenised sample was kept for two hours in a boiling water bath (sample temperature maintained at 80 °C) with occasional shaking. After 2 h, the solution was cooled down to room temperature and another 200 mL of deionized water was added (the final volume was 500 mL). The final homogenised sample was filtered using Whatman 41 filter paper. Finally, an aliquot sample containing from 5 to 50 mg of $NaNO_2$ (typically 5 mL of the filtered sample) was transferred into a 50 mL volumetric flask and mixed with 2.5 mL of the sulfanilamide reagent 0.375 w/v containing 15% (v/v) of acetic acid. The mixture was left to rest for 5-10 minutes at room temperature to allow completion of the diazotization process. Then, 2.5 mL of 0.133 w/v naphthylethylenediamine (NED) coupling reagent containing 15% (v/v) of acetic acid were also added. Afterwards, the reacting mixture was diluted to volume (50 mL volumetric flask), mixed and left in a dark environment for another 15 min until colour development. The absorbance of the sample was measured at 540 nm against a reagent blank [2, 3]. The nitrite content was calculated, following the Beer's law, using the formula:

$$\text{Sample } NaNO_2 = c \text{ x } \frac{50}{a} \text{ x } \frac{500}{s}$$

where sample $NaNO_2$ is µg $NaNO_2$ /g sample; *c* is the concentration (in ppm) of $NaNO_2$ (from the standard curve); *a* is the aliquot size (mL); *s* is the sample weight (g).

S4–9. Preliminary electrochemical characterisation of HMT-PMBI/NGNP coated electrodes.

First of all, the ratio of HMT-PMBI and NGNPs utilized to make the composite material was optimized considering several factors such as good dispersion, stability over time and the need of maintaining the background (capacitive) currents at the minimum (Figures not shown). The optimum nanocomposite ratio was found to be 1% wt. HMT-PMBI and 0.25 % wt. NGNPs. This composition of the HMT-PMBI/NGNP composite was used throughout all experiments. Firstly, the CVs of the composite coated electrode in the presence of the redox mediator, $IrCl_6^{2-}$ were recorded. Figure S4 shows the cyclic voltammograms of 5 mM K_2IrCl_6 at a bare, HMT-PMBI and HMT-PMBI/NGNP coated electrodes with the appearance of the typical redox peaks of the couple Ir(IV)/Ir(III). For all three electrodes, the peak-to-peak separation is higher than 59 mV indicating a diffusion-controlled process. The cyclic voltammograms show also the typical behavior of ionomers deposited on electrode surface, e.g. the oxidation process is facilitated and occurring at less positive potential for HMT-PMBI (0.62 V) than the bare GCE electrode (0.66 V).

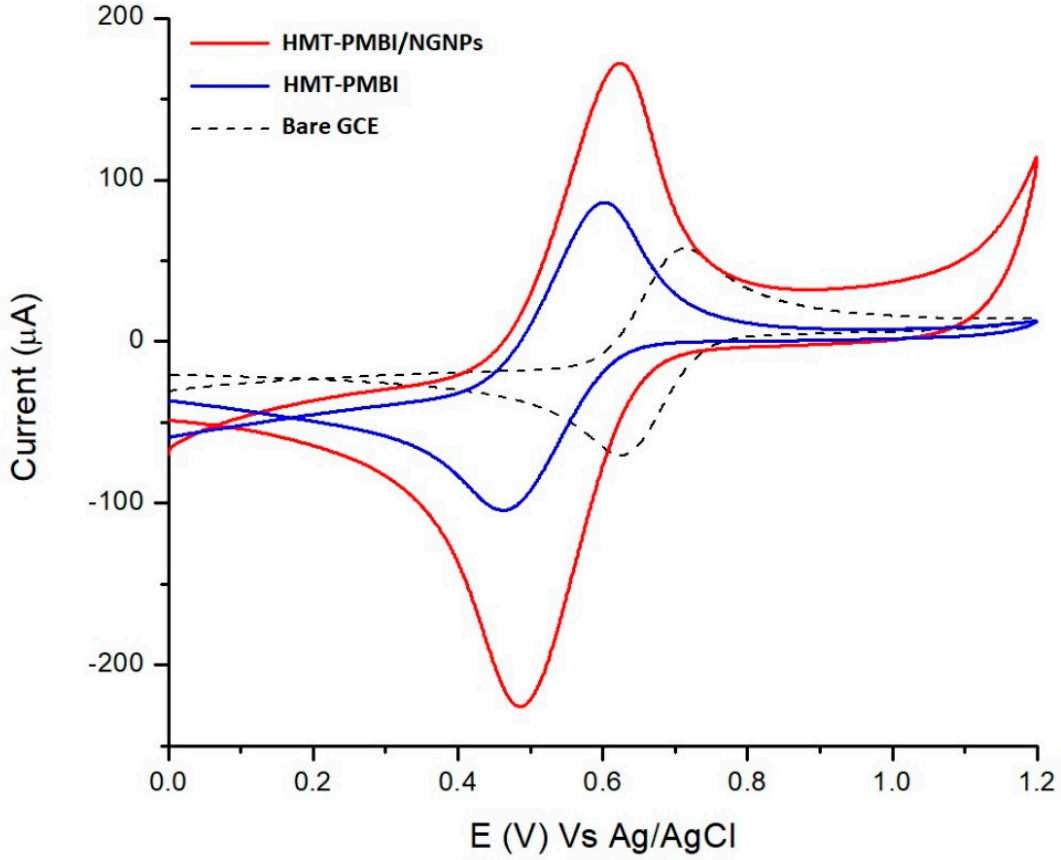

Figure S4. Cyclic voltammograms of 5 mM of $IrCl_6^{2-}$ at a bare GCE, a HMT-PMBI and a HMT-PMBI/NGNP coated electrode in 0.1 M NaCl supporting electrolyte. Scan rate 0.1 V s^{-1}.

At the same time, the magnitude of the peak current at the HMT-PMBI coated electrode is 1.5 times that one recorded at the GCE electrode. As expected, the addition of NGNPs to the ionomer causes a significant increase of the peak current (from 80 µA for the bare GCE to 175 µA for HMT-PMBI/NGNP coated electrode) as an indication of the facile electron transfer, but also the result of the larger electroactive area that arises for the presence of electrically-conductive NGNPs. The preconcentration capabilities of the film were further analyzed by transferring the modified electrode, previously loaded with the redox mediator, into a solution containing only the supporting electrolyte (0.1 M NaCl). The redox mediator was strongly retained inside the modified electrode (Figure S5) where the peak current only decreases by 22% compared with the CVs performed under loading conditions, from a value of 193 µA to 150 µA.

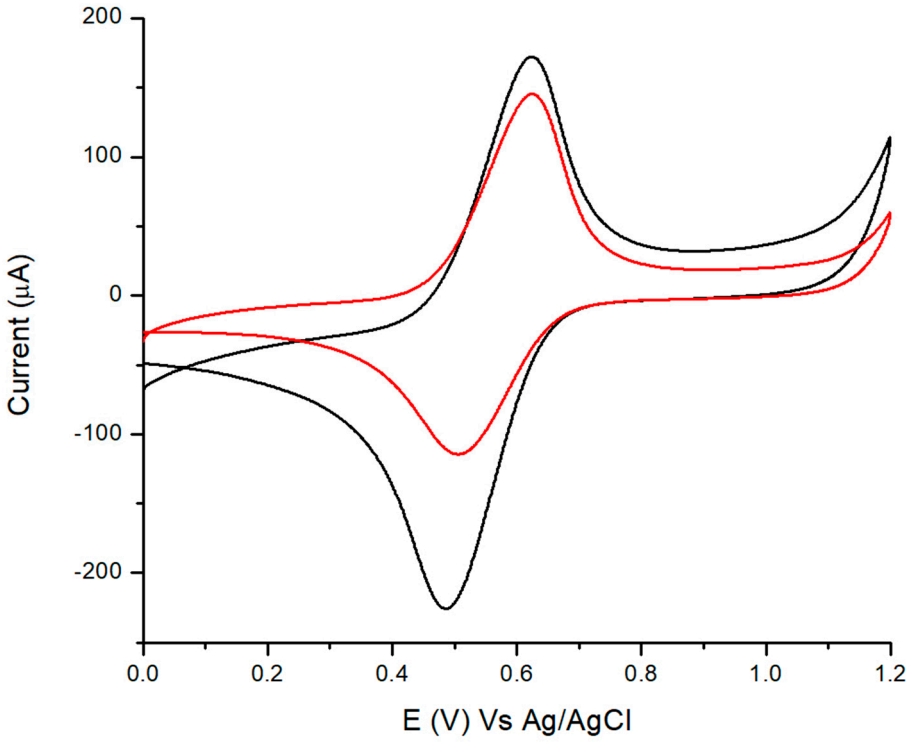

Figure S5. Cyclic voltammograms of 5 mM of $IrCl_6^{2-}$ at a HMT-PMBI/NGNP coated electrode in 0.1 M NaCl supporting electrolyte (black curve) and after transferring (red curve) to 0.1 M NaCl supporting electrolyte. Scan rate 0.1 V s^{-1}.

The retention time of the redox mediators inside the film was studied by recording several cyclic voltammograms of 5 mM K_2IrCl_6 in 0.1M NaCl supporting electrolyte at the HMT-PMBI and HMT-PMBI/NGNP coated electrodes. Figure S6(a-b) showed the CVs obtained at HMT-PMBI/NGNP and HMT-PMBI coated electrodes, respectively, loaded in 5 mM K_2IrCl_6, then transferred in only supporting electrolyte and continuously cycled. As the cycling time increased (from 1 minute to 1 hour), the peak currents decrease as a result of the diffusion of the redox mediator from the coated film to the solution.

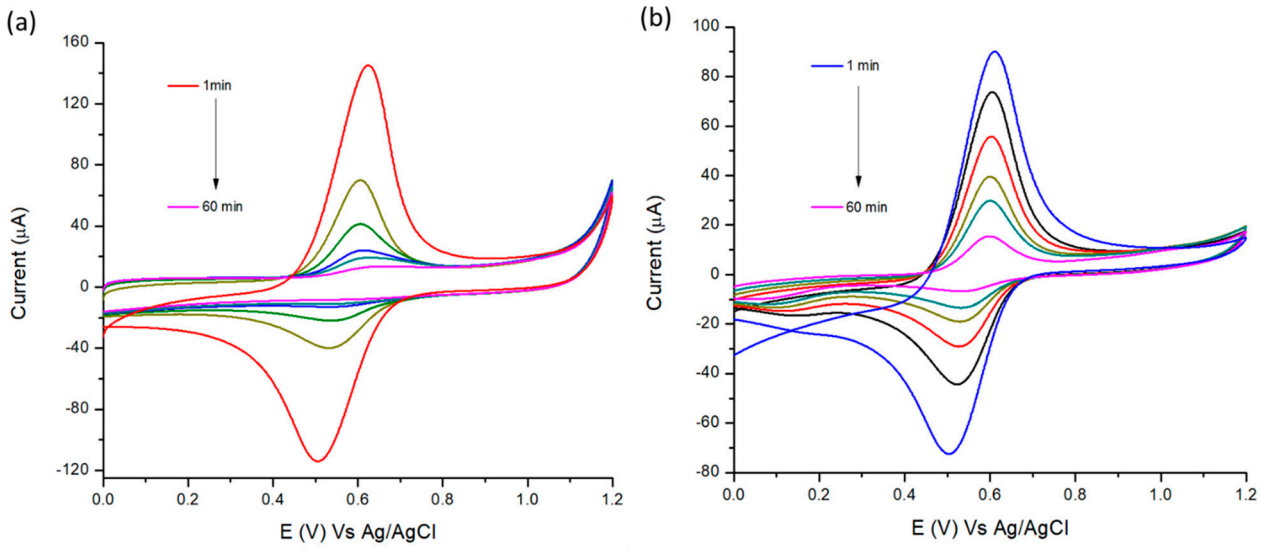

Figure S6. Cyclic voltammograms of 5 mM of $IrCl_6^{2-}$ at HMT-PMBI/NGNP (a) and HMT-PMBI (b) coated electrodes recorded at different times under conditions of continuous cycling. Before the experiment, the coated electrodes were fully loaded in 5 mM K_2IrCl_6 solution. Supporting electrolyte, 0.1 M NaCl; scan rate 0.1 V s^{-1}.

These results indicate a more pronounced loss of $IrCl_6^{2-}$ at the HMT-PMBI/NGNP coated electrode, compared to the HMT-PMBI coated electrode. This is likely to be due to the introduction of defects in the composite film after adding bulky NGNPs, which then eased the diffusion of $IrCl_6^{2-}$ from the composite film to the solution. After incubating the HMT-PMBI/NGNP coated electrode in a 5 mM $IrCl_6^{2-}$ solution for 5 min, the cyclic voltammograms obtained in a 0.1 M NaCl supporting electrolyte at different potential scan rate show two different behaviour. At low scan rates ($v < 50$ mV s^{-1}, S7(a, c)) the peak current intensity varies linearly with the scan rate and, under these circumstances, the ΔE_p value is lower than 59 mV as expected for a Nernstian process. This behaviour is typical of a thin-layer or surface-controlled process. A thin-layer process is operative when the polymer layer is thinner than the concentration gradient of the redox species, hence, the transition from thin-layer to diffusion-control is also thickness-dependent [4, 5].

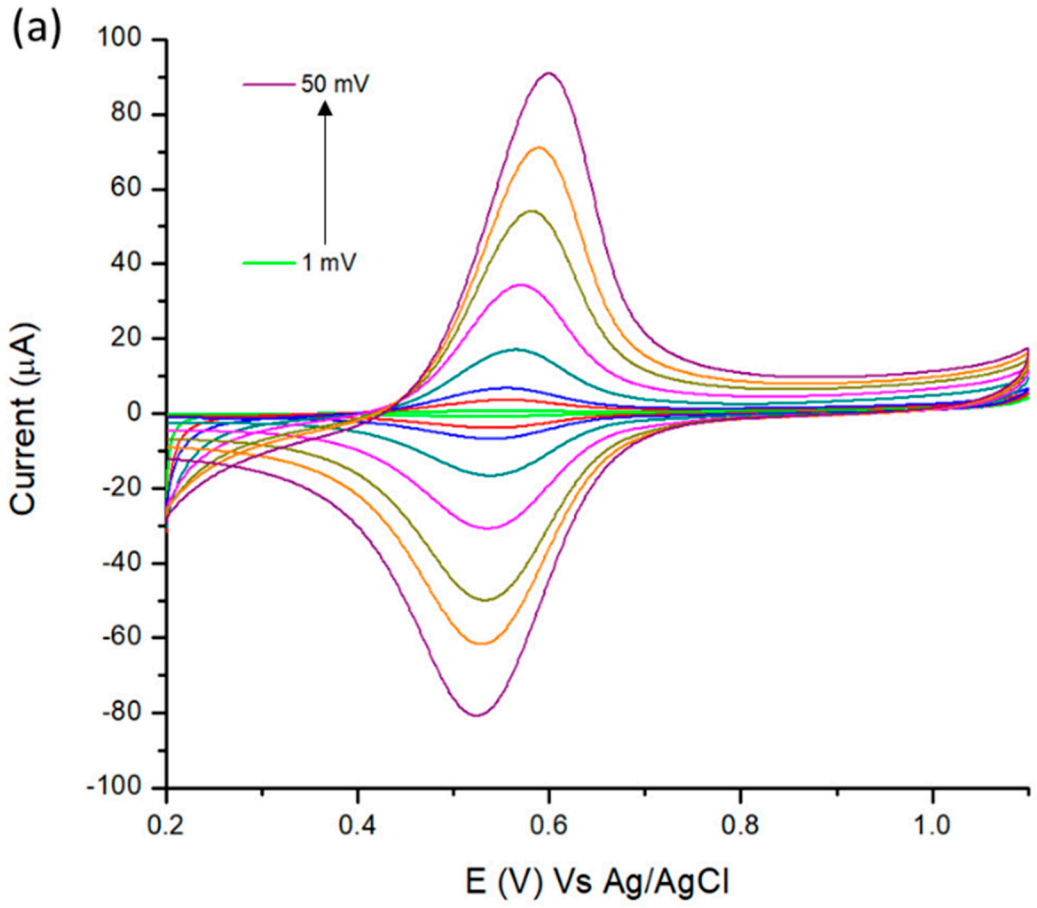
(a)
50 mV
1 mV
Current (μA)
E (V) Vs Ag/AgCl
100
80
60
40
20
0
-20
-40
-60
-80
-100
0.2
0.4
0.6
0.8
1.0

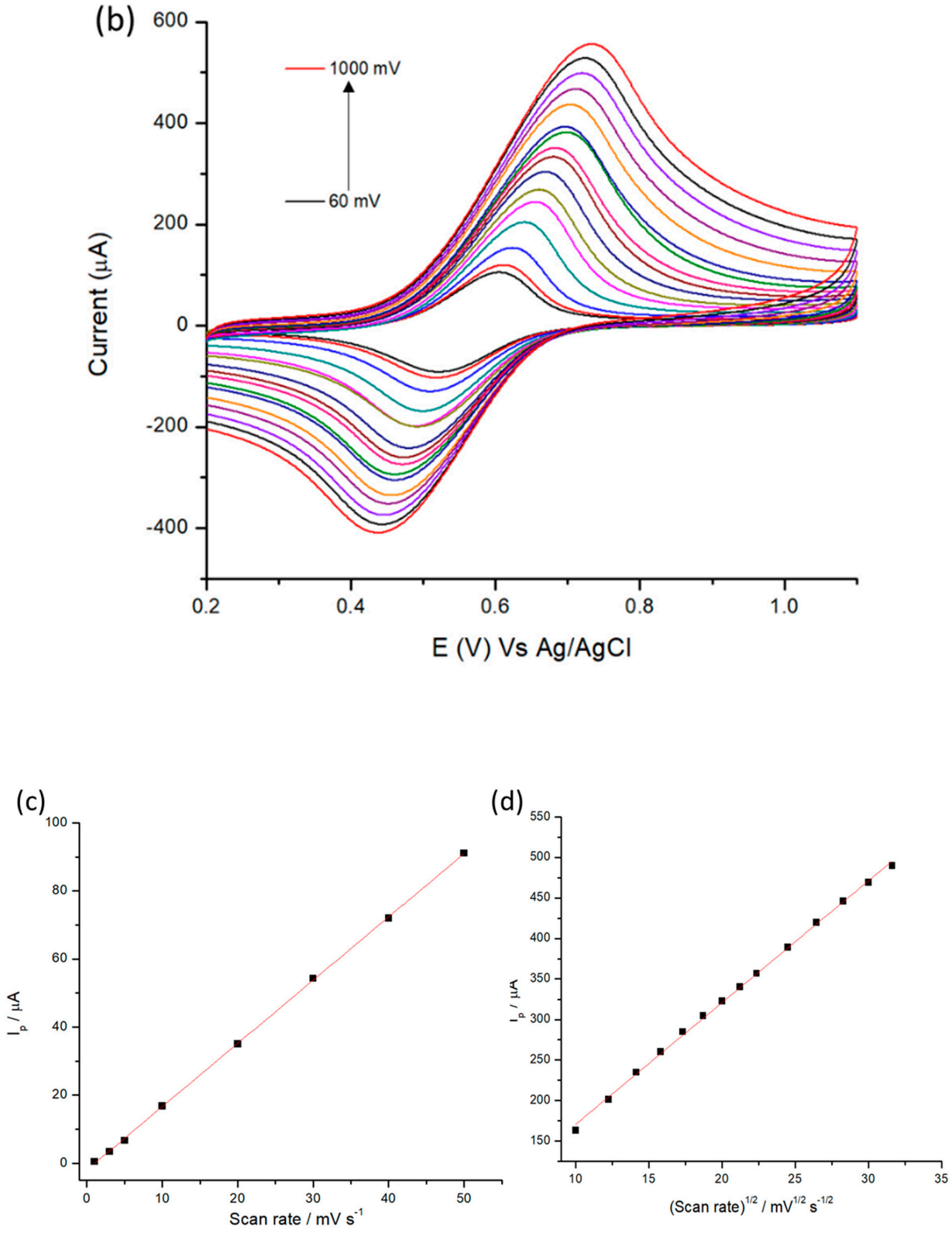

Figure S7. Cyclic voltammograms of 5 mM of $IrCl_6^{2-}$ at HMT-PMBI/NGNP coated films after transferring to 0.1 M NaCl supporting electrode. Scan rates from (a) 1 mV s^{-1} to 50 mV s^{-1} and (b) 60 mV s^{-1} to 1000 mV s^{-1}. Plot of the anodic peak currents *vs.* the scan rate (c) and *vs.* the square root of scan rate (d).

In addition, the peak currents recorded at higher scan rates (v > 50 mV s^{-1} (S7(b, d)) varies linearly with the square root of the scan rate, indicating a diffusion-controlled process. To note that the transition from thin-layer to diffusion-control occurs at higher scan rates for HMT-PMBI/NGNPs compared to HMT-PMBI (Figure not shown) as an indication of the higher apparent diffusion coefficient (D_{app}) of the redox mediator in HMT-PMBI/NGNP coated electrodes. It is possible to calculate the charge and with the knowledge of the film thickness, to estimate the concentration of the redox species incorporated within the film. The apparent diffusion coefficient, D_{app}, provides information about the diffusion of the analytes through the film and are calculated using the following procedure. Firstly, the surface coverage values (Γ/ mol cm^{-2}) of the composite films are calculated from CVs of coated electrodes previously loaded with the redox probe and displaying thin-layer characteristics (the coated electrode are transferred to the electrolyte solution with no redox specie) using the relation:

$$\Gamma = Q/nFA$$

where Q (C) is the charge measured on the forward or reverse scan, n is the number of electrons transferred, A (cm^2) is the surface area of the electrode and F is the Faraday constant (96486 C mol^{-1}). With the knowledge of the film thickness, Φ, obtained with the profilometer, it is possible to express this value as the concentration of the redox mediator, C_p, using the relation:

$$C_p = \Gamma/\Phi$$

To estimate the diffusion coefficient, we plotted the anodic peak current, I_p versus the square root of the scan rate, $v^{1/2}$, and applied the Randles-Sevčik equation [6]:

$$i_p = 0.4463 \left(\frac{F^3}{RT}\right)^{1/2} n^{3/2} A {D_O}^{1/2} C_O^* v^{1/2}$$

with the tacit assumption that the redox process is reversible as well as diffusion controlled.

In the case of HMT-PMBI/NGNPs the introduction of graphite nanoplatelets leads to an increase of the effective electrode area, hence the use of the geometric area is not possible. In order to estimate the effective surface area, we have applied the integrated Cottrell's equation (named also Anson's equation) using chronocoulometry:

$$Q_d = \frac{2nFAD^{\frac{1}{2}}C_o t^{\frac{1}{2}}}{\pi^{\frac{1}{2}}}$$

By plotting Q_d vs. $t^{1/2}$ it is possible to extrapolate the value of the effective surface area, using a value of D as $(8.2 \pm 0.4) \times 10^{-6}$ cm^2 s^{-1} [7]. The results obtained are summarised in Table S5.

As the introduction of NGNPs in the coating leads to an increase of the electroactive surface area of the electrode, we calculated the effective area of the electrode using the Anson's (chronocoulometric) method [8]. The results show that the effective area of the HMT-PMBI/NGNP coated electrode was 4-fold higher than that of the geometric area of a bare GCE (see Table S8(a)).

Table S8(a). Slope values obtained from the converted chronocoulometric plot and the corresponding calculated surface area.

Electrode	Graph slope (**A/V$^{1/2}$ s$^{-1/2}$**)	Surface area (cm^2)
Bare GCE	1.01x10^{-4}	0.064 ± 0.01
HMT-PMBI (1%)	1.48x10^{-4}	0.094 ± 0.02
HMT-PMBI/NGNPs 1%	4.0x10^{-4}	0.25 ± 0.07

Table S8(b) summarizes the thickness, electrode area, surface coverage, concentration of the redox mediator within the composite film, and D_{app} values evaluated using the procedure described in S8. The calculated D_{app} values for the $Ir^{3+/4+}$ redox couple using the Randles–Sevcik equation were found to be 9.57 x 10^{-7} cm^2·s^{-1} for the HMT-PMBI/NGNP coated electrodes with a standard deviation of 0.56 x 10^{-7} cm^2·s^{-1} (N=5). This value is one order of magnitude higher than that calculated for the HTM-PMBI coated electrodes.

Table S8(b). Parameters extracted using cyclic voltammetry and chronocoulometry relating HMT-PMBI and HMT-PMBI/NGNPs coated electrodes loaded in 5mM K_2IrCl_6 after transferring to 0.1M NaCl; Φ = film thickness, Γ = surface coverage and Cp = concentration of K_2IrCl_6 in the film.

Electrode	Φ /μm	A / cm^2	Γ / mol cm^{-2}	C_p / mol dm^{-3}	D_{app}/ cm^2 s^{-1}
Bare GCE	N/A	0.064 ± 0.01	N/A	5 x 10^{-3}	8.2 x 10^{-6}
HMT – PMBI	2.83 ± 0.35	0.094 ± 0.02	(1.42 ± 0.26) x 10^{-8}	(5.03 ± 1.4) x 10^{-2}	(5.73 ± 1.16) x 10^{-8}
HMT – PMBI / NGNPs	8.92 ± 0.32	0.25 ± 0.07	(5.68 ± 1.4) x 10^{-9}	(6.37 ± 1.8) x 10^{-3}	(9.57 ± 0.56) x 10^{-7}

It is important to point out that the D_{app} is not only dependent on the physical diffusion of the redox mediators, but also depends on the self-exchange (electron hopping) between redox couples, which of course is enhanced when the electrically conductive NGNPs are added to the polymer. [9, 10]. It is important to note that in using such method we have made the assumptions that (i) the film is uniform, (ii) the polymer does not swell during the experiment and (iii) the redox behavior is fully reversible and (iv) the process is diffusion-controlled. The permselectivity of the modified electrode, *e.g.* the ability of the coating composite film to repel species of same charge was also ascertained by loading the coated electrodes with a positively charged redox mediator such as $Ru(NH_3)_6^{3+}$. Figure S9 shows the cyclic voltammograms of 3 mM of $Ru(NH_3)_6^{3+}$ at a bare GCE, HMT-PMBI and HMT-PMBI/NGNP coated electrodes. As expected, both HMT-PMBI and HMT-PMBI/NGNP coated electrodes do not show any voltammetric peak related to the redox behavior of the $Ru(NH_3)_6^{3+}$ as a proof that the positively charged benzimidazolium groups (see S2) of HMT-PMBI and NGNPs are effective in repelling the positively charged ruthenium redox specie.

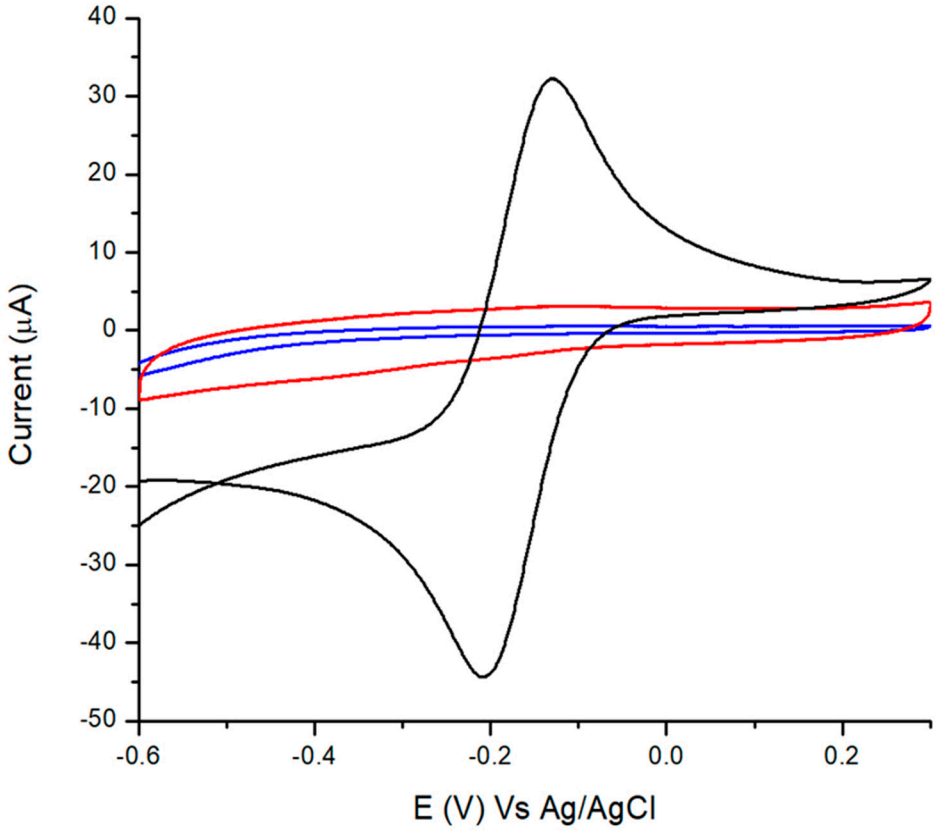

Figure S9. Cyclic voltammograms of 3 mM of $Ru(NH_3)_6^{3+}$ at a bare GCE (black line), HMT-PMBI (blue line) and HMT-PMBI/NGNP (red line) coated electrodes using supporting electrolyte, 0.1 M NaCl; scan rate 0.1 V s^{-1}.

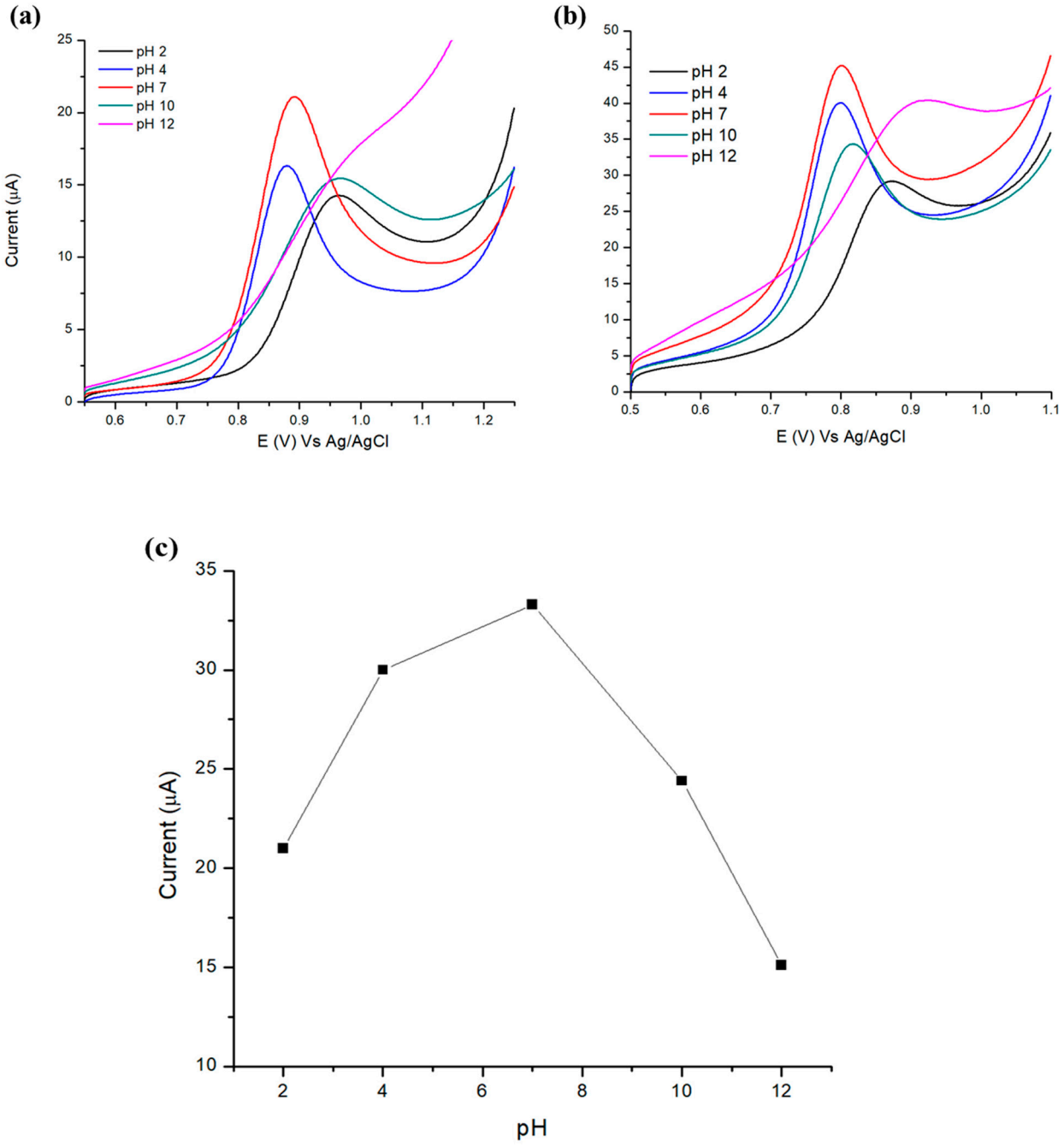

Figure S10. Linear sweep voltammograms of 200 μM nitrites at different pH values, at a (a) HMT- PMBI and (b) HMT-PMBI/NGNPs coated electrodes; supporting electrolyte 0.1 M NaCl; scan rate 0.1 V s^{-1}. (c) Plot of anodic peak current at different pH for HMT-PMBI/NGNPs coated electrodes.

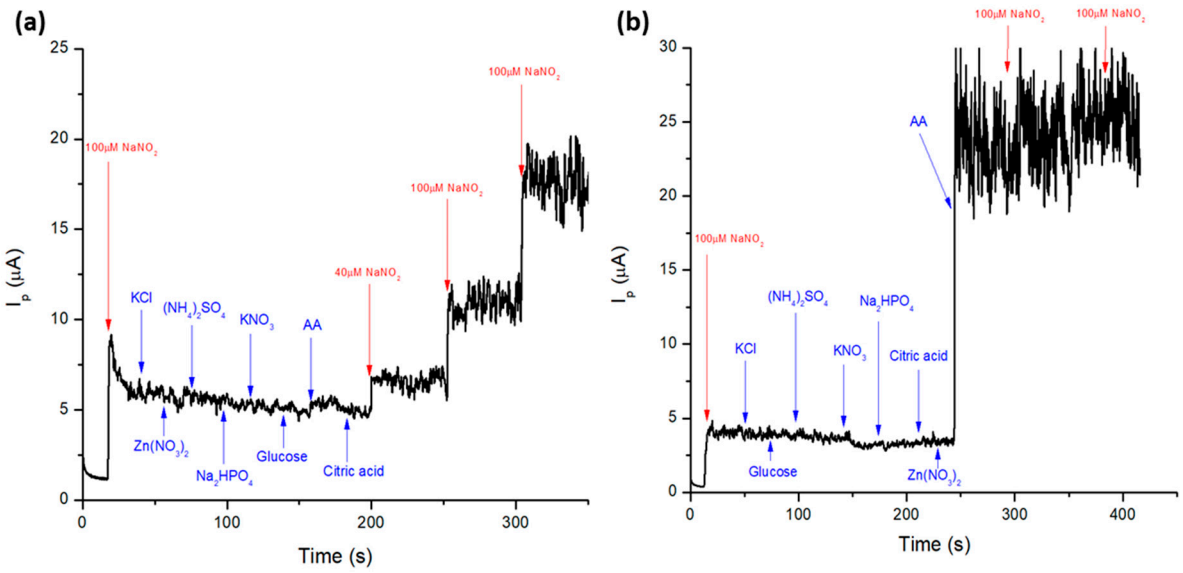

Figure S11. Chronoamperometric response of different nitrite concentrations at (a) 0.86 V applied to a HMT-PMBI/NGNP coated electrode, (b) 1 V applied to a bare GCE in the presence of interfering species and a 0.1 M NaCl supporting electrolyte (b) Chronoamperometric (i-t) response of bare GCE, applied potential 1 V; other conditions as in (a). The concentration of the interferences in the solution is 10 mM.

Table S12. Time required for the extraction of nitrites for each meat/water ratio.

Sample	Amount of bacon (g)	Deionised water (mL)	Size Duran glass bottle (mL)	Meat/Water Ratio (g/mL)	Microwave time (s)
A	5	100	150	0.05	90
B	5	200	250	0.025	210
C	5	400	500	0.0125	340

Table S13. Estimated concentration of nitrites calculated using the Beer's law. The meat/water ratio corresponds to the quantity of water used during the heating process.

Sample	Sample	Meat/Water	Calculated Nitrite content (**µg $NaNO_2$ /g Bacon Meat)**			
		(g/mL)	Sample 1	Sample 2	Sample 3	**Mean**
Microwave	A	0.05	1.96	2.03	1.89	1.96 ± 0.07
	B	0.025	3.43	4.05	3.36	3.61 ± 0.38
	C	0.0125	5.27	5.88	4.93	5.36 ± 0.48
ISO		0.1	5.44	5.51	5.74	5.56 ± 0.15
AOAC		0.0167	5.44	5.92	5.5	5.62 ± 0.26

Table S14. Analytical performances of HMT-PMBI/NGNP coated electrode for the detection of nitrite in bacon solution.

Method	Added (µM)	Found (µM)	Recovery %
CV	-	0.83 ± 0.16	-
	1	2.0 ± 0.24	109.3
CA	-	0.87 ± 0.11	-
	1	1.92 ± 0.17	102.7

Table S15. Recent Analytical performances of amperometric sensors for the detection of nitrite ions.

Electrode	Linear Range NO_2^- (µM)	LoD NO_2^- (µM)	Technique	Reference
Ag nanosilver/H-C_3N_4 on carbon cloth	5 – 1000	0.216	CA	*[11]*
FeSe nanorods on carbon cloth	0.625-6775	0.07	CA	*[12]*
Co phopshide NPs/3D phosphorous/nitrogen co-doped carbon frameworks	0.01 -1.184	0.005	DPV	*[13]*
Au NPs decorated bimetallic CuNi/GCE	50-1150	0.017	CA	*[14]*
SnO_2/Pt/Ti/SiO_2/Ti	10-400	1.7	CA	*[15]*
Graphene oxide functionalised imidazole rings	1-1000	0.28	SWV	*[16]*
RGO/$MnFe_2O_4$/PANI/GCE	0.05-12000	0.015	DPV	*[17]*
PEDOT/PEDOT-SH/Au NPs/ITO	150-1000 and 1000-1600	0.051	CA	*[18]*
polyNiCo/GCE	2.49-1700	0.45	CA	*[19]*
rGO/MoS_2/PEDOT/GCE	1-1000	0.059	DPV	*[20]*
Air annealing carbon fibre paper (OCFP)	0.1-3838	0.07	CA	*[21]*
Cu/CBSA/GCE	0.5-500	0.1	DPV	*[22]*
AuNPs/MoS_2 nanoflowers/GN/GCE	5-5000	1	CA	*[23]*

$NiFe_2O_4$/CPE	0.1-1000	0.1236	CA	*[24]*
TPQPCl/GCE	1-500	1.07	CA	*[25]*
HMT-PMBI/NGNP/GCE	1-300	0.64	CA	This work

Note: RGO = reduced graphene oxide; PANI = polyaniline; PEDOT = Poly(3,4-ethylenedioxythiophene); ITO = indium tin oxide; CBSA = crosslinked bovine serum albumin; TPQPCl = tris(2,4,6-trimethoxyphenyl)polysulfone-methylene quaternary phosphonium chloride

References

1. ISO, *Determination of nitrite content, ISO 2918:1975 standard*, in *International Standards Meat and Meat Product*. 1975: Genèva, Switzerland: International Organization for Standarization.
2. AOAC, *Nitrites in cured meat. Colorimetric method AOAC 973.31-1996*. 1997.
3. Mohamed, A.A., et al., *Modification of AOAC Method 973.31 for Determination of Nitrite in Cured Meats.* Journal of AOAC INTERNATIONAL, 2019. **91**(4): p. 820-827.
4. Ugo, P. and L.M. Moretto, *Ion-exchange voltammetry at polymer-coated electrodes: Principles and analytical prospects.* 1995. **7**(12): p. 1105-1113.
5. Ugo, P. and L.M. Moretto, *Ion Exchange Voltammetry*, in *Ion Exchange Technology I: Theory and Materials*, I. Dr and M. Luqman, Editors. 2012, Springer Netherlands: Dordrecht. p. 403-435.
6. Bard, A.J. and L.R. Faulkner, *Electrochemical methods: fundamentals and applications, Second Edition*. Vol. 2. 2001: Wiley New York.
7. Bard, A.J. and J. Ketelaar, *Encyclopedia of Electrochemistry of the Elements.* Journal of The Electrochemical Society, 1974. **121**(6): p. 212C.
8. Buttry, D.A. and F.C. Anson, *Effects of electron exchange and single-file diffusion on charge propagation in Nafion films containing redox couples.* Journal of the American Chemical Society, 1983. **105**(4): p. 685-689.
9. Ruff, I. and V.J. Friedrich, *Transfer diffusion. I. Theoretical.* The Journal of Physical Chemistry, 1971. **75**(21): p. 3297-3302.
10. Dahms, H., *Electronic conduction in aqueous solution.* The Journal of Physical Chemistry, 1968. **72**(1): p. 362-364.
11. Shen, Y., et al., *Nanosilver and protonated carbon nitride co-coated carbon cloth fibers based non-enzymatic electrochemical sensor for determination of carcinogenic nitrite.* Science of The Total Environment, 2020. **742**: p. 140622.
12. Zhe, T., et al., *In situ preparation of FeSe nanorods-functionalized carbon cloth for efficient and stable electrochemical detection of nitrite.* Sensors and Actuators B: Chemical, 2020. **321**: p. 128452.
13. Zhu, D., et al., *A free-standing and flexible phosphorus/nitrogen dual-doped three-dimensional reticular porous carbon frameworks encapsulated cobalt phosphide with superior performance for nitrite detection in drinking water and sausage samples.* Sensors and Actuators B: Chemical, 2020. **321**: p. 128541.
14. Lei, P., et al., *Gold nanoparticles decorated bimetallic CuNi-based hollow nanoarchitecture for the enhancement of electrochemical sensing performance of nitrite.* Microchimica Acta, 2020. **187**(10): p. 572.

15. Lete, C., et al., *Nitrite electrochemical sensing platform based on tin oxide films.* Sensors and Actuators B: Chemical, 2020. **316**: p. 128102.
16. Tajiki, A., et al., *Voltammetric Detection of Nitrite Anions Employing Imidazole Functionalized Reduced Graphene Oxide as an Electrocatalyst.* **n/a**(n/a).
17. Sahoo, S., et al., *Interfacial polymerized RGO/MnFe2O4/polyaniline fibrous nanocomposite supported glassy carbon electrode for selective and ultrasensitive detection of nitrite.* Sensors and Actuators B: Chemical, 2020. **309**: p. 127763.
18. Ge, Y., et al., *Electrochemical synthesis of multilayered PEDOT/PEDOT-SH/Au nanocomposites for electrochemical sensing of nitrite.* Microchimica Acta, 2020. **187**(4): p. 248.
19. Islam, T., et al., *Fabrication of Ni–Co-Based Heterometallo-Supramolecular Polymer Films and the Study of Electron Transfer Kinetics for the Nonenzymatic Electrochemical Detection of Nitrite.* ACS Applied Polymer Materials, 2020. **2**(2): p. 273-284.
20. Madhuvilakku, R., et al., *Glassy carbon electrodes modified with reduced graphene oxide-MoS2-poly (3, 4-ethylene dioxythiophene) nanocomposites for the non-enzymatic detection of nitrite in water and milk.* Analytica Chimica Acta, 2020. **1093**: p. 93-105.
21. Zhu, W., et al., *Surface Engineering of Carbon Fiber Paper toward Exceptionally High-Performance and Stable Electrochemical Nitrite Sensing.* ACS Sensors, 2019. **4**(11): p. 2980-2987.
22. Sun, C., et al., *An electrochemical sensor for nitrite using a glassy carbon electrode modified with Cu/CBSA nanoflower networks.* Analytical Methods, 2019. **11**(39): p. 4998-5006.
23. Han, Y., et al., *Sensitive electrochemical sensor for nitrite ions based on rose-like AuNPs/MoS2/graphene composite.* Biosensors and Bioelectronics, 2019. **142**: p. 111529.
24. Nithyayini, K.N., M.N.K. Harish, and K.L. Nagashree, *Electrochemical detection of nitrite at NiFe2O4 nanoparticles synthesised by solvent deficient method.* Electrochimica Acta, 2019. **317**: p. 701-710.
25. Jones, T.R., et al., *Tris(2,4,6-trimethoxyphenyl)polysulfone-methylene quaternary phosphonium chloride (TPQPCl) ionomer chemically modified electrodes: An electroanalytical study towards sensing applications.* Electrochimica Acta, 2019. **311**: p. 160-169.